Journal of Superconductivity: Incorporating Novel Magnetism, Vol. 14, No. 1, 2001

Harmonic Balance Algorithms for the Nonlinear Simulation of HTS Devices

C. Collado,[1] J. Mateu,[1] J. Parrón,[1] J. Pons,[1] J. M. O'Callaghan,[1] and J. M. Rius[1]

This paper describes the application of Harmonic Balance algorithms to predict nonlinear effects in planar High Temperature Superconductors (HTS) microwave circuits. The resulting algorithms are fast and efficient and can be used both for the characterization of the nonlinearities in the HTS material, and for the prediction of the behavior of an HTS circuit given the parameters of these nonlinearities (such as a dependence of the surface impedance on the current density). Most previously published nonlinear HTS models can be used, because the algorithms are not restricted to a specific model of HTS nonlinearities. Two different types of algorithms are described: (1) algorithms specific for one-dimensional resonators (transmission lines and TM_{010} disk resonators) and (2) an algorithm based on the combination of Method of Moments and Harmonic Balance, applicable to 2D planar structures with few restrictions in their shape. Several cross-checks with theory and measurements are presented.

KEY WORDS: Superconductivity; nonlinearity; Harmonic Balance; intermodulation distortion; Method of Moments.

1. INTRODUCTION

High Temperature Superconductors (HTS) are being used for planar, high-selectivity microwave filters. The combination of low-loss and low-volume of these filters makes them attractive with respect to those made with other filter technologies, such as cavity-based filters. The high quality factors (Q) achieved in small, planar HTS resonators are at the heart of these advantageous features. However, the combination of high Q and small sizes also results in high current densities being produced in these resonators. Many evidences [1–4] already exist indicating that high current densities in HTS materials produce nonlinear effects, such as degradation of quality factors in resonators, and generation of signals at spurious frequencies. These nonlinear effects are distributed, and may be characterized by a HTS surface impedance dependent on the current density ($Z_s(J)$). As a result, the performance of filters and other HTS devices is highly dependent on material parameters ($Z_s(J)$) and on the shape of the resonators within the device, which affects the current densities in the HTS materials. Predicting the performance of these devices requires not only the knowledge of $Z_s(J)$, but also methods to evaluate how this parameter combines with the distributed electromagnetic behavior of the device. This paper presents several of these methods, some of which are specific of the resonator topologies currently used in microwave HTS devices.

All the methods presented apply a common technique (Harmonic Balance) [5] of calculating the nonlinear effects. This technique is being widely used in circuit simulations of lumped nonlinear devices. Its effectiveness is due to the independent calculation of linear effects in frequency domain, and nonlinear effects in time domain. The methods presented in this paper use this technique in distributed structures (planar microwave HTS resonators and filters) instead of circuits with lumped components, where Harmonic Balance is usually applied.

Generation of spurious signals is one of the most troublesome effects of nonlinearities in HTS filters, specially intermodulation products whose

[1]Department of Signal Theory and Communications, Universitat Politecnica de Catalunya, Barcelona 08034, Spain.

0896-1107/01/0200-0057$19.50/0

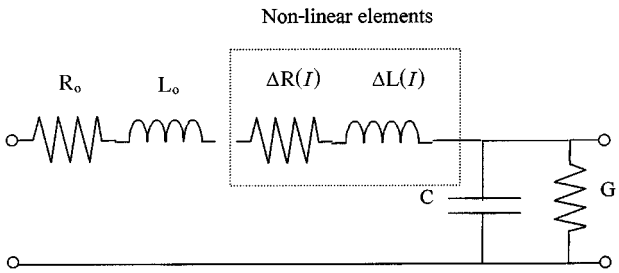

Fig. 1. Equivalent circuit of an infinitesimal section of a transmission line. The elements $\triangle R(I)$ and $\triangle L(I)$ account for the nonlinearities in the HTS.

frequencies may be close to the bandpass of the filter. Many of the recent works in modeling microwave HTS nonlinearities are geared toward quantifying intermodulation products [6,7]. The methods presented here are well-suited to simulate such effects. To illustrate this, the examples and cross-checks described focus on third-order intermodulation products on HTS resonators. However, the methods are quite general and are not restricted to resonant conditions, nor to the typical two-tone harmonic signals used to produce intermodulation spurious.

2. NONLINEAR SIMULATION OF HTS TRANSMISSION LINES

2.1. Model

Transmission lines in the form of microstrip, stripline, or coplanar waveguide are currently used in HTS microwave devices. The nonlinear effects of HTS in these lines can be modeled by using a distributed RLCG model (Fig. 1) in which the resistance and inductance per unit length at a point along the line are dependent on the total current at that point [6].

$$\begin{aligned} L(I) &= L_0 + \Delta L(I) \\ R(I) &= R_0 + \Delta R(I) \end{aligned} \tag{1}$$

As detailed in [6], the nonlinear terms $\triangle L(I)$ and $\triangle R(I)$ can be derived from the properties of the material. In [6], this is done from the dependence of the penetration depth on the current density ($\lambda(J)$), but $Z_s(J)$ may be used instead.

The response of a HTS nonlinear transmission line to a large-signal source can be analyzed by forming a circuit containing a cascade of many identical cells, such as the one in Fig. 1, and other elements that may be connected to the line, such as a resistive load, reactive elements used for coupling, and the source (Fig. 2). The circuit in Fig. 2a can then be modeled as shown in Fig. 2b, that is, as a linear network with $N+1$ ports loaded with a source at one of its ports, and N identical nonlinear elements at the remaining ports.

To analyze the intermodulation products and other spurious generated in the HTS line, we assume that the source in Fig. 2 is producing currents at frequencies ω_1 and ω_2, and that the impedance matrix ($\mathbf{Z}$) of the $(N+1)$-port is found at ω_1, ω_2, and all other frequencies where spurious signals may exist ($2\omega_1 - \omega_2, 2\omega_2 - \omega_1, 3\omega_1, 3\omega_2, \ldots$ etc).

2.2. Algorithm

The algorithm (Fig. 3) uses the currents through the nonlinear elements as state variables, which are stored in a vector $\mathbf{I}_{NL}$ containing the currents at each element and each frequency. An initial estimate of the components in this vector is made by assuming that the voltage drop across the N nonlinear elements is

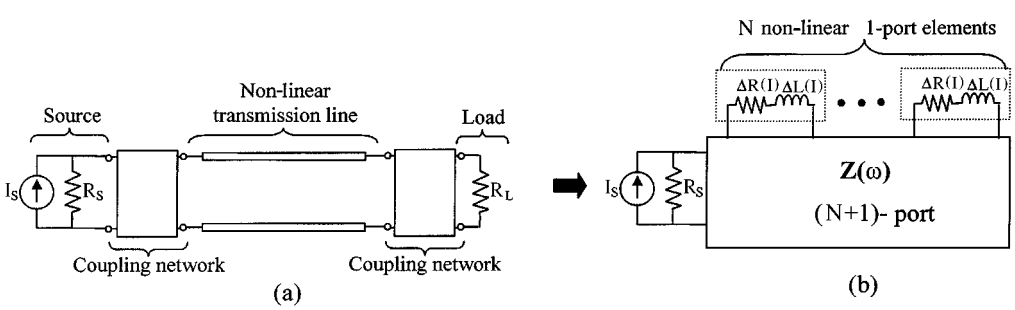

Fig. 2. Equivalent circuit of a HTS (nonlinear) transmission line consisting of a linear network with $N+1$ ports loaded with N nonlinear 1-ports.

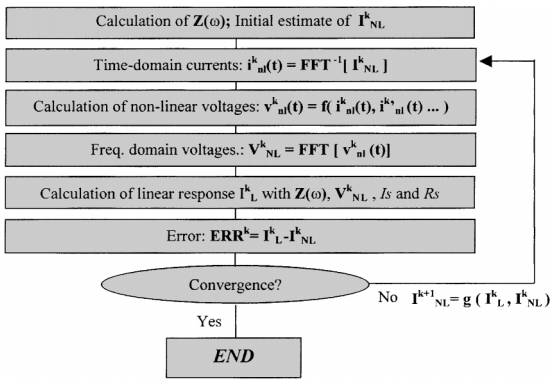

Fig. 3. Flow diagram of the Harmonic Balance algorithm used (MHB).

zero. With this assumption, the current flowing out of the linear network and impressed on the N nonlinear elements can be found by solving a linear problem involving only the linear $(N+1)$-port and the source Is (Fig. 2b). Next, $\mathbf{I}_{\mathrm{NL}}$ is transformed into time domain so that the voltage drops along the N nonlinear elements can be found using both the current, its first derivative, and $\triangle L(I)$ and $\triangle R(I)$. These voltages are then transformed to frequency domain and a vector $\mathbf{V}_{\mathrm{NL}}$ is formed, which contains the voltages generated by each of the N nonlinear elements, at each frequency of interest. By applying these voltages at the ports of the linear $(N+1)$-port, one can find a new vector of currents $\mathbf{I}_{\mathrm{L}}$. If this vector of currents is not sufficiently close to the present estimate of $\mathbf{I}_{\mathrm{NL}}$, a refined estimate can be formed by jointly taking into account the present estimate of $\mathbf{I}_{\mathrm{NL}}$, and its corresponding $\mathbf{I}_{\mathrm{L}}$. There are several methods of making this estimate. One simple approach is to make $\mathbf{I}_{\mathrm{NL}}^{k+1} = p \cdot \mathbf{I}_{\mathrm{NL}}^{k} + (1-p) \cdot \mathbf{I}_{\mathrm{L}}^{k}$ [8] and set the parameter p between 0 and 1. Slow, safe convergence is achieved for high values of p, whereas fast—and potentially unstable—convergence rates result for p close to 0.

Once the new estimate for $\mathbf{I}_{\mathrm{NL}}$ is calculated, the iteration is restarted by calculating $\mathbf{V}_{\mathrm{NL}}$ and its corresponding $\mathbf{I}_{\mathrm{L}}$. This process ends when no significant differences are found between $\mathbf{I}_{\mathrm{NL}}$ and $\mathbf{I}_{\mathrm{L}}$.

The efficiency of the algorithm can be enhanced by taking advantage of the sparsity in $\mathbf{Z}$, which results from the high translation symmetry in the $(N+1)$-port that models the transmission line as a cascade of identical cells. We refer to this algorithm as "Multiport Harmonic Balance" (MHB) to distinguish it from the standard Harmonic Balance applied to a few nonlinear elements.

2.3. Tests

Numerical tests have been performed to compare the MHB results with those obtained from closed-from equations derived in [6] for a half-wave line resonator. These equations are derived assuming a quadratic dependence of $L(I)$ and $R(I)$, and give the maximum current level of the intermodulation spurious $(2\omega_1 - \omega_2)$ as a function of the parameters of the line and the current in the excitation source. Specific values of $L(I)$ and $R(I)$ for a HTS microstrip line with no grain boundaries or other defects can also be inferred from this reference. Using this information, the current distribution of Fig. 4 is obtained. The current levels in this figure deviate fractions of a percent over the theoretical predictions in [6] which include some approximations), proving that the algorithm is giving correct results.

2.4. Possible Uses

As opposed to [6], where a square-law dependence is assumed for $L(I)$ and $R(I)$, MHB is not restricted to a specific type of HTS nonlinearities, and almost any type of functional dependence can be used in $L(I)$ and $R(I)$. This is a valuable feature because currently there is no consensus on the functional behavior that Z_{s} has on J (or equivalent dependences, like $\lambda(J)$) [9–11], and this translates to several possible functional dependences of the inductance and resistance per unit length (L, R) on the current flowing through the line (I). Hence, the flexibility of MHB might prove valuable in two aspects: (1) The determination of $L(I)$, $R(I)$, and/or $Z_{\mathrm{s}}(J)$ corresponding to the specific HTS samples being used and (2) The simulation of circuits made with these specific samples. The following sections describe our ongoing work in these two directions.

3. NONLINEAR SIMULATION OF TM_{010} DISK RESONATORS

Current distributions in planar HTS transmission lines have sharp peaks along their edges [12,13]. This enhances the nonlinear effects in planar HTS line resonators and makes these effects highly sensitive to the morphology and material properties of the line edges, which may be degraded because of the fabrication process, or difficult to reproduce from sample

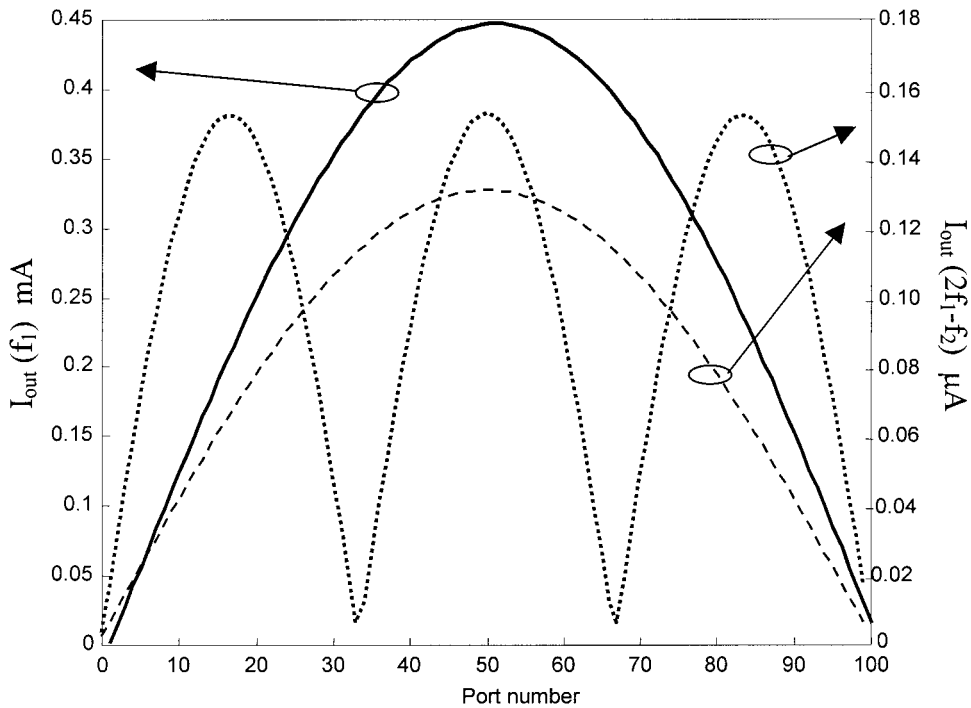

Fig. 4. Current distribution of fundamental (continuous), intermodulation (dashed), and third harmonic (dotted) modes along a half-wave line resonator calculated with MHB. Line parameters (both linear and nonlinear) are inferred from [6]. Agreement with closed-form equations in [6] is within 1%.

to sample. TM_{010} disk resonators have been shown to circumvent these problems [14,15] and are being used in several HTS devices [16].

The intermodulation distortion in a disk resonator is analyzed in [17]. Assuming a specific dependence of $\lambda(J)$, closed-form equations are derived for predicting the current density of the third order spurious. The analysis is done treating the resonator as a radial transmission line, and finding a radially dependent capacitance and inductance per unit length. That analysis makes MHB applicable to TM_{010} disk resonators with only minor modifications: the $(N+1)$-port in Fig. 2 is still formed by a cascade of cells such as the one if Fig. 1, but the values of the elements in these cells are not identical; instead, they vary to account for the dependence of the capacitance and inductance per unit length on the radius. The advantage of using MHB is that the nonlinear analysis is possible for types of material nonlinearities different from those postulated in [17]. Numerical tests similar to those made in the previous section have been performed with satisfactory results. Further cross-checks will be shown in Section 6.

4. MHB IN THE DETERMINATION OF MATERIAL NONLINEARITIES

One of the difficulties in obtaining reliable information on the material nonlinearities ($Z_s(J)$ or equivalent) from experimental data stems from the complicated dependence of the experimental observables (power of spurious signals, degradation of quality factors, etc.) with $Z_s(J)$ or $\lambda(J)$. The MHB algorithms being developed can be of great help in this type of problem, because—when fully developed—these should be sufficiently fast to simulate the test resonators and perform an iterative adjustment of $Z_s(J)$ to match simulation results with experimental observables.

As a preliminary proof of this type of function, MHB has been used to reproduce the intermodulation measurements in [9]. The nonlinearity in the inductance per unit length ($L(I)$) of the line has been adjusted to fit the data in Fig. 3 of [9] (no nonlinearities were assumed in the resistance per unit length in [9]). In [9], the dependence of $L(I)$ with I at low powers was assumed to follow a square-law, and to change to a dependence of $L(I)$ on the absolute value of I at

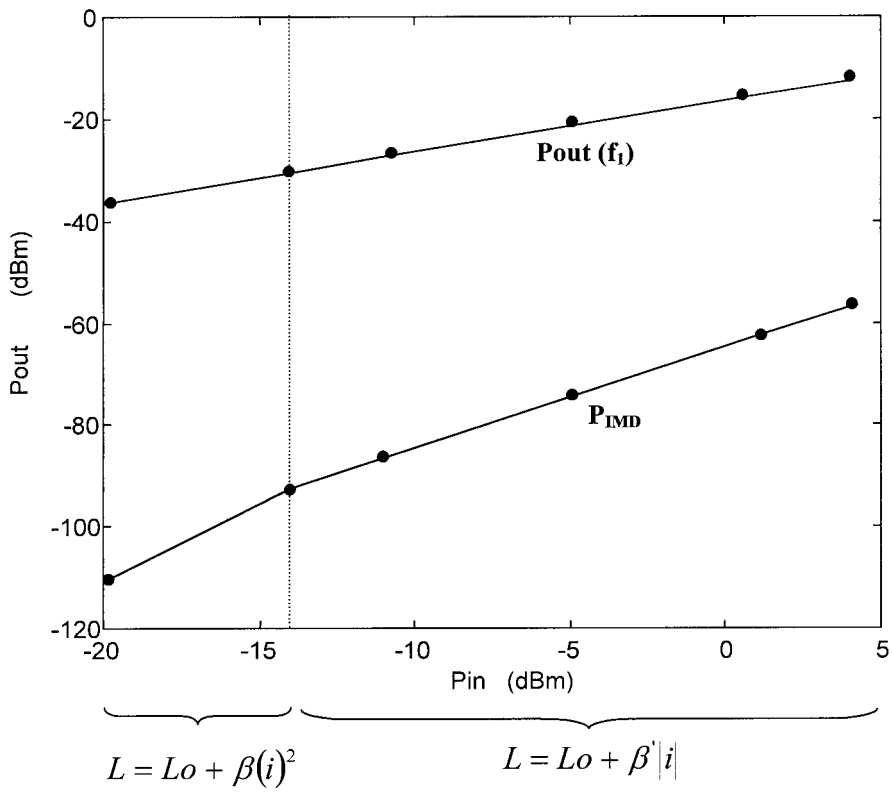

Fig. 5. P_{out} vs. P_{in} curve for the symmetric mode (current in both arms in the same direction) of the hairpin resonator measured in [9]. Solid lines are MHB fits and dots are measured values.

high power levels. Figure 5 (of this work) shows the results of the MHB adjustment: a 3 : 1 slope is obtained in the square-law region, whereas the observed 2 : 1 slope is obtained at higher power levels. In both regions, the MHB results (line) match measured values (dots). Furthermore, the power of the intermodulation products in the square-law region obtained in our simulation is in very close agreement with the theoretical prediction made in [6] (Eq. 33 in that reference).

Similar results can be obtained by fitting MHB simulations to measurements of disk resonators.

5. HTS NONLINEAR CIRCUIT SIMULATOR

The results of Sections 2 and 3 are being combined to produce a netlist-based circuit simulator capable of handling HTS nonlinear lines and disk resonators, together with other circuit elements such as capacitors, inductors, resistors, impedance inverters, etc. The nonlinearities in the HTS transmission lines are defined by entering $L(I)$, $R(I)$, and the equivalent parameters for TM_{010} disk resonators. The program can accept almost any mathematical function for $L(I)$ and $R(I)$. This simulator allows single or double-frequency sources, enabling the calculation of intermodulation products and other spurious in HTS filters. The simulator is capable of finding the spatial distribution of voltages and currents along the various resonators of a filter, at any of the frequencies of interest (fundamental and spurious frequencies) and for a given source power. It is also capable of sweeping the power and/or frequency(es) of the source and find the voltage/current at any point within the filter as a function of frequency or power. For illustration purposes, Figs. 6 and 7 show a simulation example, where a 9 pole forward-coupled filter is simulated. The nonlinearities in the HTS lines are assumed to be those outlined in [6] (due only to the intrinsic nonlinearities of YBCO). As shown in Fig. 6, intermodulation products are found to be highest at the bandpass edges, which is in good qualitative agreement with measurements made on other HTS filters [18].

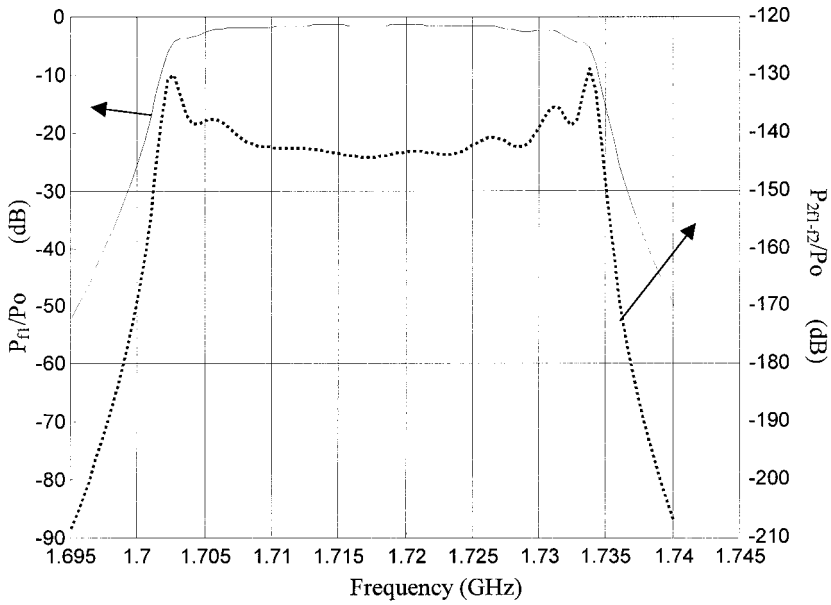

Fig. 6. Frequency response of a forward-coupled 9 pole filter showing the transfer function at the fundamental frequency, and the frequency dependence of the third-order intermodulation product normalized to the power of the source. The frequency difference of the two tones applied to the filter is kept constant at 500 KHz.

6. SIMULATION OF TWO-DIMENSIONAL HTS STRUCTURES

Simulating the nonlinear behavior of HTS planar structures without restricting their shape is possible by combining Harmonic Balance and the Method of Moments (MoM). A simple qualitative description of this method is possible by taking advantage of the parallelisms between this method and the one used in Section 2.

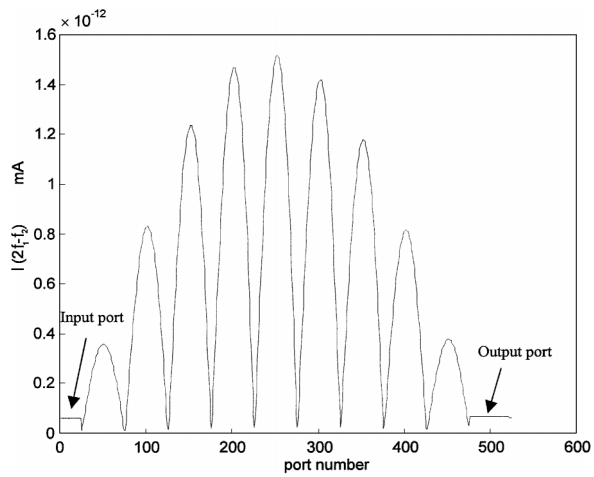

Fig. 7. Spatial distribution of the intermodulation currents along the various resonator of a forward-coupled 9 pole filter. Frequencies are kept 500 KHz apart and close to the edge of the passband, to maximize intermodulation products.

The MoM allows the use of matrix equations to relate, at a given frequency, the surface currents at a mesh of points on the superconductor (**J**) to the incident electric field **E** (i.e., that produced by the signal source in the absence of metallic or superconducting structures) [19]:

$$\mathbf{E} = \mathbf{ZJ} \tag{2}$$

The matrix **Z** takes into account the linear part of the superconductor's surface impedance and the field scattered by **J**. Equation (2) is equivalent to the matrix **Z** of the linear $(N+1)$-port in Fig. 2, and has to be determined at a number of different frequencies where fundamental and spurious fields may exist.

The nonlinearities in the superconductor may be described in time domain by an equation relating the electric fields (e_{nl}) and current densities at the superconductor surface (j):

$$e_{\mathrm{nl}} = \triangle R_{\mathrm{s}}(j) \cdot j + \triangle L_{\mathrm{s}}(j) \frac{\partial j}{\partial t} \tag{3}$$

where $\triangle R_{\mathrm{s}}(0) = 0$ and $\triangle L_{\mathrm{s}}(0) = 0$, that is, the electric fields in Eq. (3) are those due only to the nonlinearities

of the superconductor, and are superimposed to those resulting from the linear surface impedance of the material. In other words, $\triangle R_s(j)$ and $\triangle L_s(j)$ are equivalent to $\triangle R(I)$ and $\triangle L(I)$ of the N nonlinear elements in Fig. 2. An iteration scheme can now be set, in terms that are analogous to those of Section 2, that is, the surface currents are used as state variables and applied to both the linear part of the problem (Eq. (2)), and to the nonlinear part (Eq. (3)). Both results are compared to produce a refined estimate of **J**, which will be used in successive iterations if it turns to be significantly different from the previous estimate.

The MoM–MHB algorithm has been applied to a superconducting TM_{010} disk resonator, to compare it with the results of the algorithm described in Section 3. Test values of surface impedance (linear and nonlinear) have been chosen and converted to resistances and inductances per unit length for the radial transmission line used in Section 3. Figures 8 and 9 show the MoM–MHB results, detailing the mesh structure and total current densities in Fig. 8, and a graph of current densities for the fundamental and third-order intermodulation product (Fig. 9). The results in Fig. 9 have been compared to those obtained with the algorithm in Section 3. There are slight differences between both methods, but it seems clear that the correct intermodulation currents are achieved if the amplitude of the fundamental signals is correct.

7. CONCLUSION

Prediction of the nonlinear effects in planar HTS resonators requires simulation techniques that take into account the distributed nature of these structures. Several algorithms using Harmonic Balance are described. Two of them are developed for specific resonator geometries (line and disc resonators), and a third one is being developed that is not restricted in the geometry of the resonator. Good agreement with theoretical results is shown for the resonator-specific algorithms, and agreement is also found when analyzing disk resonators with the general algorithm.

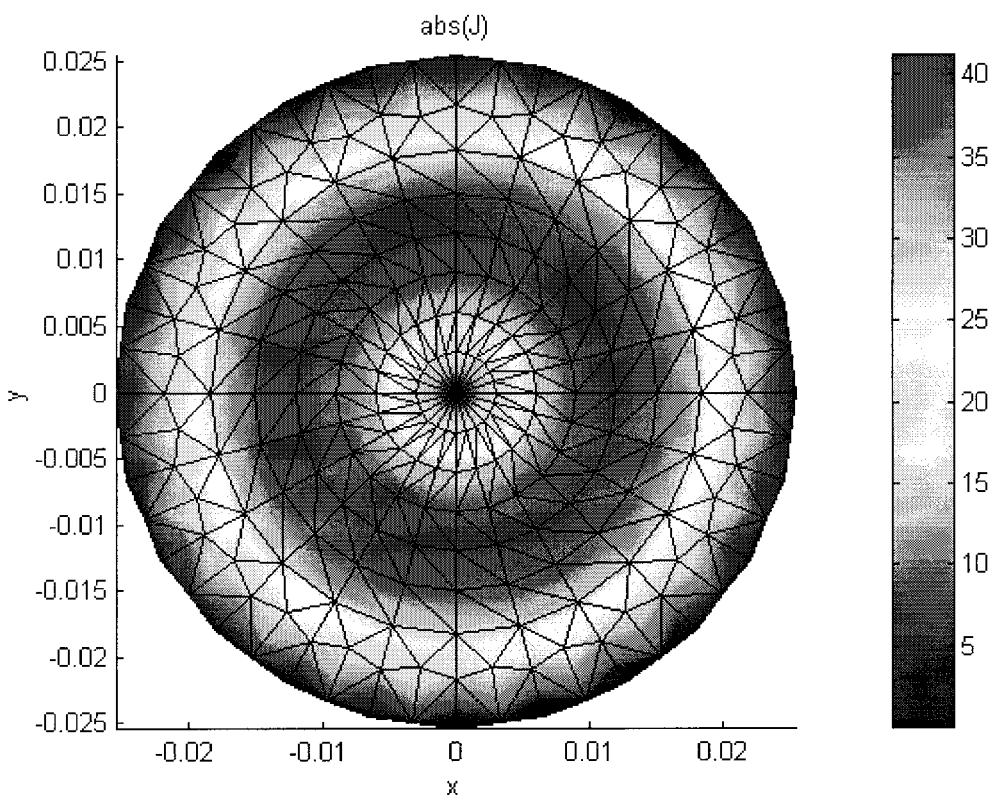

Fig. 8. Plot of the intermodulation current density in a TM_{010} disk resonator calculated with the MoM–MHB algorithm. The mesh used in the calculations is also shown.

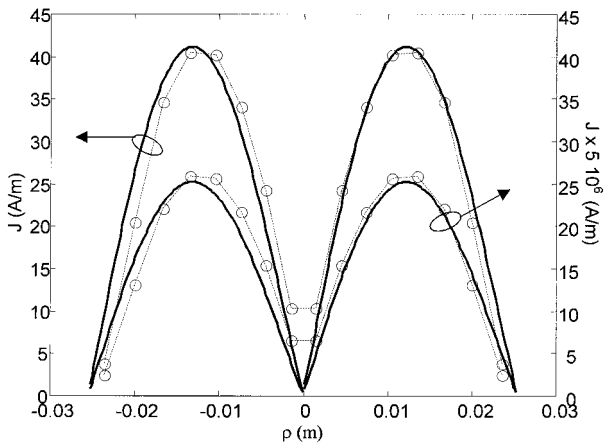

Fig. 9. Comparison of distribution of current density of the TM_{010} disk resonator simulations made with Mom–MHB (circles indicate actual simulated points; dashed lines are used to interpolate) and the radial transmission line method of Section 3 (continuous lines). The left column shows the fundamental values, and the right column shows the third-order intermodulation products.

These algorithms can be applied to the experimental extraction of nonlinearities of HTS materials, and preliminary examples are given.

ACKNOWLEDGMENTS

This work was funded by the Spanish Ministry of Education and Culture through projects MAT-0984-C03-03 and TIC 98-1037 and scholarship AP99-78085980, and by the Generalitat de Catalunya through scholarships 1997 FI 00679.

REFERENCES

1. D. E. Oates, A. C. Anderson, D. M. Sheen, and S. M. Ali, *IEEE Trans. Micr. Theory Tech.* **39**(9), 1522–1529 (1991).
2. P. P. Nguyen, D. E. Oates, G. Dresselhaus, and M. S. Dresselhaus, *Phys. Rev. B* **48**(9), 6400–6413 (1993).
3. J. H. Oates, R. T. Shin, D. E. Oates, M. J. Tsuk, and P. P. Nguyen, *IEEE Trans. Appl. Supercond.* **3**(1), 17–22 (1993).
4. B. Avenhaus, A. Porch, M. J. Lancaster, S. Hensen *et al.*, *IEEE Trans. Appl. Supercond.* **5**(2), 1737–1740 (1995).
5. S. A. Maas, *Nonlinear Microwave Circuits* (Artech House, 1988).
6. T. Dahm and D. J. Scalapino, *J. Appl. Phys.* **81**(4), 2002–2008 (1997).
7. O. G. Vendik, I. B. Vendik, and T. B. Samoilova, *IEEE Trans. Micr. Theory Tech.* **45**(2), 173–178 (1997).
8. R. G. Hicks and P. J. Khan, *Electron. Lett.* **16**(10), 375–376 (1980).
9. B. A. Willemsen, T. Dahm, and D. J. Scalapino, *Appl. Phys. Lett.* **71**(26), 3898–3900 (1997).
10. B. A. Willemsen, K. E. Kihlstrom, and T. Dahm, *Appl. Phys. Lett.* **74,** 753–755 (1999).
11. T. Dahm, D. J. Scalapino, and B. A. Willemsen, *J. Supercond.* **12,** 339–342 (1999).
12. M. A. Hein, C. Bauer, W. Diete, S. Hensen, T. Kaiser, G. Miller, and H. Piel, *J. Supercond.* **10,** 109–120 (1997).
13. R. B. Hammond, E. R. Soares, B. A. Willemsen, T. Dahm, D. J. Scalapino, and J. R. Schrieffer, *J. Appl. Phys.* **84**(10), 5662–5667 (1998).
14. H. Chaloupka, M. Jeck, B. Gurzinski, and S. Kolesov, *Electron. Lett.* **32,** 1735–1736 (1996).
15. S. Kolesov, H. Chaloupka, A. Baumfalk, and T. Kaiser, *J. Supercond.* **10**(3), 179–187 (1997).
16. A. C. Anderson, H. Wu, Z. Ma, P. A. Polakos, P. M. Mankiewich *et al.*, *IEEE Trans. Appl. Supercond.* **9**(2), 4006–4009 (1999).
17. T. Dahm, D. J. Scalapino, and B. A. Willemsen, *J. Appl. Phys.* **86**(7), 1–4 (1999).
18. T. Yoshitake and S. Tahara, *Appl. Phys. Lett.* **67**(26), 3963–3965 (1995).
19. R. F. Harrington, *Field Computation by Moment Methods* (Macmillan, New York, 1968).